Fibers and Polymers 2016, Vol.17, No.3, 469-476
DOI 10.1007/s12221-016-5798-z

ISSN 1229-9197 (print version)
ISSN 1875-0052 (electronic version)

Modeling and Optimization of Dynamic Puncture Behaviors for Flexible Inter-/Intra- Reinforced Compound Fabrics

Ting-Ting Li[1,2], Rui Wang[1], Ching-Wen Lou[3], Jan-Yi Lin[4], Mei-Chen Lin[4], and Jia-Horng Lin[4,5,6]*

[1]*School of Textiles, Tianjin Polytechnic University, Tianjin 300387, China*
[2]*Tianjin and Education Ministry Key Laboratory of Advanced Textile Composite Materials, Tianjin Polytechnic University, Tianjin 300387, China*
[3]*Institute of Biomedical Engineering and Material Science, Central Taiwan University of Science and Technology, Taichung 40601, Taiwan*
[4]*Laboratory of Fiber Application and Manufacturing, Department of Fiber and Composite Materials, Feng Chia University, Taichung 40724, Taiwan*
[5]*School of Chinese Medicine, China Medical University, Taichung 40402, Taiwan*
[6]*Department of Fashion Design, Asia University, Taichung 41354, Taiwan*
(Received November 1, 2015; Revised December 31, 2015; Accepted February 20, 2016)

Abstract: In this article, the new model of dynamic puncture behaviors of intra-/inter- reinforced compound fabrics which are fabricated by nonwovens and reinforced fabrics using needle-punching and thermal bonding technique is constructed by the maximum deformation and stress-wave transmission theory. Moreover, the number of layers for E1 puncture protection is optimized based on numerical analysis of penetration depth. Dynamic puncture model shows that the dynamic puncture resistance depends on elastic modulus of reinforced fabrics, deformation radius and thickness of compound fabrics. The maximum puncture resistance and penetration depth both have parabola relations to number of layers. This study provides the accurate prediction model of puncture force and safety layers for designing puncture-resisting body armor in the future.

Keywords: Puncture, Model, Optimization, Fabric, Needling, Thermal

Introduction

Flexible puncture-resistant materials are demanded for a variety of applications, such as industrial protective clothing, needle-resistant garments, racing gloves and motor suits, and ruggedized soft carriers [1]. One of the challenges is flexible puncture-resistant body armor. This study explores an intra-/inter- reinforcement to improve the fiber fraction in compound fabrics using needle punching and thermal bonding techniques. Therein, the fabric was inserted between nonwovens as reinforcement. The compound fabrics should resist against puncture weapons damage during non-uniform velocity penetration. Dynamic drop-tower puncture is used to simulate those puncture resisting properties.

The dynamic puncture resistance properties of compound fabrics can be characterized according to the National Institute of Justice (NIJ) Standard 0115.00. Three weapons, engineered knife blade P1, S1 and spike are used in this test, and the spike is chosen in this study. The drop mass mounted on the load cell, and then penetrated through the target on a prescribed stack of foams and elastomers that provide a damped target response similar to that placed on a human torso [1]. To reach E1 (24 J) protection level, the drop mass fell on the certain height and then the penetration should be less than 7 mm. In this study, the sample targets are placed on the holder with 60 mm opening in the center. After testing, the maximum dynamic puncture force and puncture depth are both evaluated to well understand the dynamic puncture properties of compound fabrics. Afterwards, the modeling based on stress-wave theory, conservation of momentum and conservation of energy are constructed on the hypothesis of elastic response for high-performance yarns (Glass, Kevlar and Carbon).

Based on the literatures, the modeling of stab resistance behaviors becomes a focus for researchers. Termonia [2] developed the first comprehensive model of static needle puncture and simulated the penetration process of needle puncture. Wang *et al.* [3] conducted the FEM model of woven fabrics and simulated the static knife penetration. Sun and Wang *et al.* [4,5] studied the static puncture behaviors of woven fabric using finite element analyses. Yahya *et al.* [6] comparatively explored the effect of impactor shapes on static puncture of woven fabric by FEM simulation. Barnat *et al.* [7] simulated the velocity, acceleration and displacement in the process of knife dynamic resistance using LSDYNA software based on the law of variation of the kinetic energy for the system. These literatures show the simulation of quasi-static stab resistance changes during testing, and the stab mostly used of the knife and flat stab weapons. Compared to above, the spike static stab resistance is a more complicated problem due to full consideration of the tightness of the fabric and the sharp profile of the puncture especially for dynamic puncture behavior. Despite Hou *et al.* [8] established the quasi-static stab resistance model based on the maximum deformation geometry after quasi-static stab testing, the tensile fracture of principle yarns becomes

*Corresponding author: jhlin@fcu.edu.tw

the main mechanism for flat stab which is different from the spike stab. As mentioned above, rare research on the modeling of the spike dynamic resistance properties of compound fabrics has done at present because of its more complicated mechanism. In daily life, sharp-pointed objects are encountered more frequently and many damages are all derived from them. Therefore, study on puncture resistance against sharp-tipped objects is more meaningful. Spike has a sharp point and easily penetrated through the space of fabrics because the radius of spike tip is smaller than that of fabric interspace. As a result, combination of fiber strength and inter-fiber friction acts to resist against the spike, of which fiber strength plays a limited effect on the spike resistance.

Moreover, an intra-/inter- structure constituting of two layers of nonwovens and one layer of woven fabric and reinforcing by needle punching and thermal bonding was proposed by us in previous study [9]. The surficial and bottom nonwovens play as the increase of the fiber content in the fabric's interspace. The new structure of compound fabrics has confirmed to be with excellent spike puncture resistance, and influences of needle punching, thermal bonding, and fiber blending as well as number of layers on spike resistance have explored by our previous experimental study [9-13]. Therefore, this study focuses on constructing spike puncture resistance models of the compound fabric based on maximum deformation and stress-wave transmission theory, intended to predict the dynamic puncture resistance force and penetration depth theoretically. The number of layers as related to penetration depth was indicated using numerical analysis to predict the minimum layers for E1 protection based on NIJ- standard. These predications can fully give the anticipation of dynamic puncture response in the future of designing the body armor which is made by flexible compound fabrics.

Experimental

Experimental Materials

Recycled Kevlar fibers (supplied by DuPont Company, America), taken from Kevlar unidirectional selvages, have a length of 50-60 mm, a fineness of 1.2 denier and 2.1 % elongation at break. High-strength Nylon 6 staple fibers (supplied by Taiwan Chemical Fiber Co. Ltd., Taiwan) were 6 denier (D) in fineness, 64 mm in length and had 10 g/d tenacity, 24.7 % elongation. Low-melting PET fibers (manufactured by Huvis Corporation, South Korea) had 4 D fineness and 51 mm length. 2 D PET fibers supplied by Far Eastern New Century Corporation, Taiwan, had 51 mm length. Three types of plain woven fabrics—glass fabric, Kevlar fabric and carbon fabric were both supplied by Jinsor-Tech Industrial Corp., and their structural parameters are listed in Table 1.

Table 1. The structural parameters of three types of fabrics

Fabric	Fineness	Weight (g/m^2)	Density (/inch)	Thickness (mm)
Glass fabric	1 K	328	34×26	0.31
Kevlar fabric	1000 D	228	28×28	0.32
Carbon fabric	12 K	390	6×6	0.60

Experimental Procedure

Kevlar/Nylon/low-melting PET nonwoven with blending ratio of 20/50/30 wt%/wt%/wt% was fabricated after nonwoven processing technology. The proportion of low-melting PET fibers was optimized as 30 wt% [14]. The weight ratio of recycled Kevlar fibers was 20 wt% as optimized by our previous study [12]. The needle-punched density was controlled as 100 needles/cm^2, and the areal weight of nonwoven was 200 g/m^2. One layer of fabric interlayered between Kevlar/Nylon/low-melting PET nonwovens was needle-punched into flexible compound fabric. Insertion of glass, Kevlar and carbon fabrics was respectively named as G-CF, K-CF and C-CF, whose compositions are displayed in Table 2. Inter-/intra- reinforcement structure of compound fabrics shows in reference [9]. Low-melting PET fibers bond among adjacent fibers and formed thermal-bonding points to achieve intra-reinforcement. The needle-punching bonds the thickness of the whole compound fabrics via vertical fibers to achieve inter-reinforcement. Through these reinforcements, the compound fabrics improved their dynamic puncture resistance properties as compared to pure fabrics.

Dynamic Puncture Property Test

Dynamic puncture test was carried out by Drop-Tower Machine (GuangNeng Machinery Co. Ltd., Taiwan) attached with PCD300A data acquisition (Sanlien Corp., Taiwan) according to NIJ Standard 0115.00. In order to achieve Protection Level 1—*E1 Strike Energy* (24 J), the spike (0.07 mm shaft radius and 24° conical angle) loaded by 2.8 kg dropped from 284 mm height onto surface of 100 mm×100 mm samples which are clamped between two square plates with 40-mm-diameter hole in the center. The

Table 2. Compositions of three kinds of compound fabrics

Name code	Upper layer	Middle layer	Bottom layer
G-CF	Kevlar/Nylon/low-melting PET nonwoven	Glass woven fabric	Kevlar/Nylon/low-melting PET nonwoven
K-CF	Kevlar/Nylon/low-melting PET nonwoven	Kevlar woven fabric	Kevlar/Nylon/low-melting PET nonwoven
C-CF	Kevlar/Nylon/low-melting PET nonwoven	Carbon woven fabric	Kevlar/Nylon/low-melting PET nonwoven

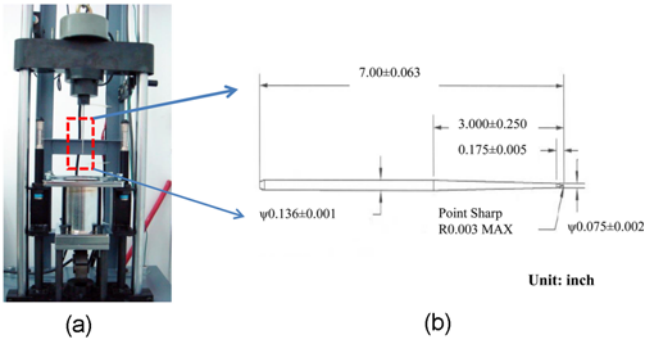

Figure 1. Instrument for dynamic puncture testing (a) and dimension of spike and (b) according to NIJ Standard-0115.00.

testing instrument and spike dimension are shown in Figure 1.

Results and Discussion

Experimental Dynamic Puncture Behaviors

The structure of intra-/inter-reinforced compound fabrics has shown in Figure 2. Nonwovens among vertical fibers inserted through interspaces among fabrics (see Figure 2(b)), forming inter-laminar reinforced structure. Therein, the nonwovens has orientation distribution (see Figure 3), and the 90 ^{o} orientation has the most staple fibers, and therefore, the surface and bottom layers of nonwovens are cross-plied to achieve the uniform fiber distribution. Thermal bonding fibers bonds among other fibers and decreases the interspace between fibers (see Figure 4), which improves the dynamic puncture resistance due to higher pushed forces to compound fabrics. Therefore, thermal bonding and vertical fibers by needle punching form intra-/inter- reinforced structure for compound fabrics.

Figure 5 shows that as time passed, dynamic puncture force increased up to the maximum value. At this moment, the puncture tip contacted with the surface of compound fabric. Then, dynamic puncture force decreases, but its slope was smaller than that of static puncture force [13]. From the dynamic puncture behavior, the time when puncture probe contacted the surface of compound fabric (t_a) has not

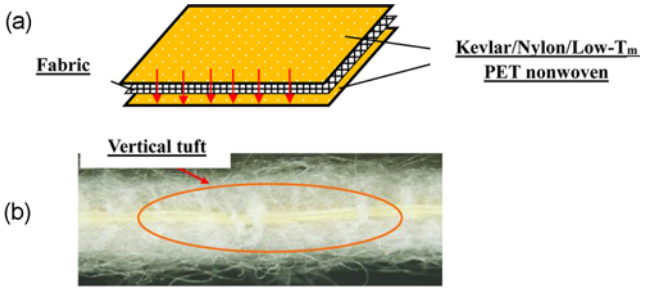

Figure 2. Structure diagram (a) and cross section (b) of compound fabrics.

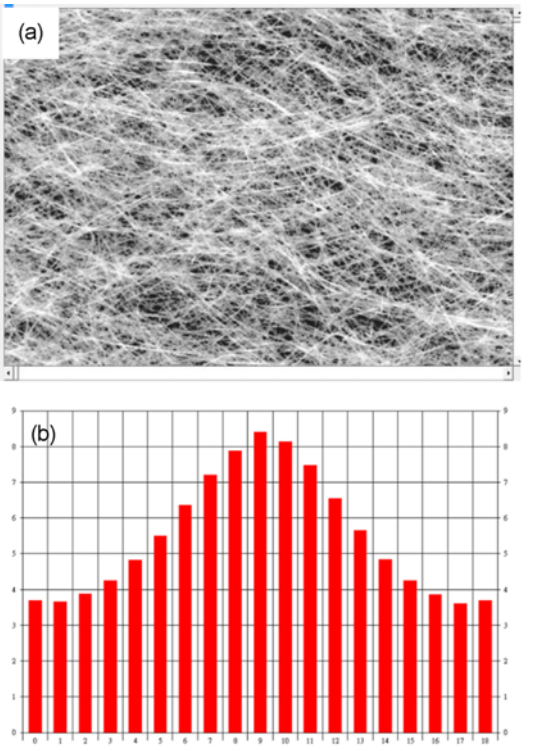

Figure 3. Surface morphology (a) and fiber orientation (b) of surficial nonwovens for compound fabrics.

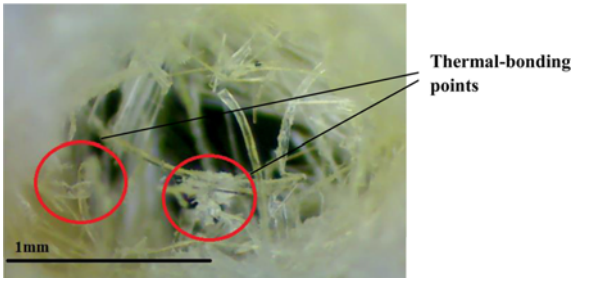

Figure 4. Thermal bonding points on the Puncture damage surface [9].

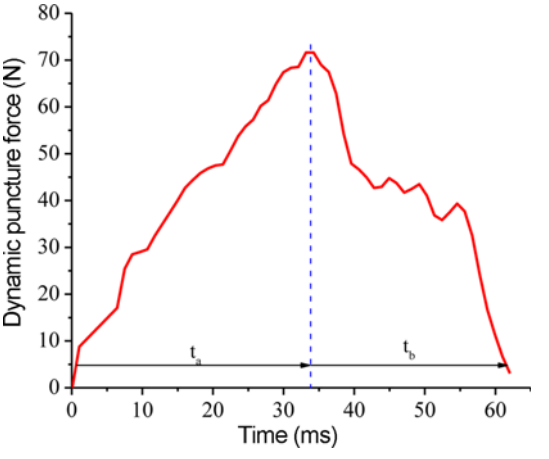

Figure 5. Dynamic puncture force vs. time characteristic curve.

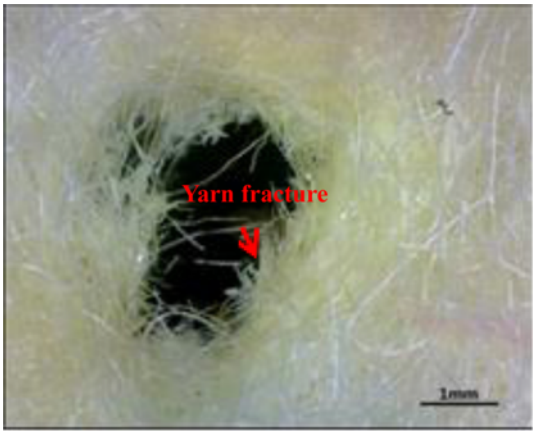

Figure 6. Damage surfaces of compound fabrics after dynamic puncture test.

significant difference between that the puncture probe penetrated through compound fabric (t_b). Compared the static puncture behavior, the friction coefficient at dynamic puncture resistance is larger than that at static puncture resistance [13]. Therefore, dynamic puncture divides into three steps: (1) Puncture begins to contact the surficial compound fabrics and then happens to be deformed; (2) Puncture penetrates through the inner of compound fabric; (3) Maximum conical radius penetrated the bottom of the compound fabrics, and the puncture starts to slow down until stop with the help of a spring.

The dynamic puncture damage is observed in Figure 6. It is found that a part of reinforced fabric is fractured, and the nonwovens are pushing aside by puncture probe. Besides, the compound fabrics are deformed periphery of damages. Therefore, the following model of dynamic puncture resistance is constructed based on the damage modes, the deformation and the fabric fracture.

Modeling of Dynamic Puncture Behavior

Through FEM simulation result in Figure 7(a), the maximum dynamic puncture resistance occurred when the maximum conical radius penetrated through compound fabrics. Therefore, the modeling of dynamic puncture behavior is based on maximum deformation. When puncture head impacted on the compound fabrics, the longitudinal and transverse waves propagated along the yarn nearby the impact point. The formed shape of compound fabric is shown in Figure 7(b). Puncture transverse wave makes the deformation radius larger, and the longitudinal wave leads to the deformation height bigger [15]. Based on wave theory, conservation of momentum and energy conservation, the prediction model of dynamic puncture force was constructed according to three steps as follow.

(1) Contacting Moment

According to conservation of momentum, the mass that

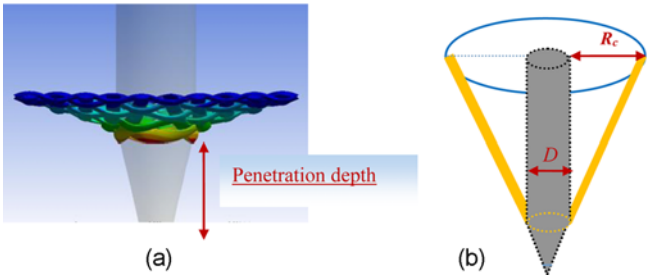

Figure 7. Fabric deformation shape by FEM simulation (a) and deformation schematic diagram (b) after puncture test.

puncture head contacts with the surface of compound fabric was:

$$m_p = \rho T_0 \pi r_{p\min}^2 \tag{1}$$

where m_p is the contacting mass between puncture head and compound fabric, r_p is the conical radius of puncture head.

Then, the mass of total system constituted of puncture head and compound is:

$$M = M_p + m_p \tag{2}$$

The moment when puncture head contacts with compound fabric complies with conservation of momentum. Then, at the contacting moment,

$$M_p V_p = (M_p + m_p) V_{p0} \tag{3}$$

The velocity of compound fabric after first momentum exchange was:

$$V_{p0} = \frac{V_p}{1+\Lambda} \tag{4}$$

where $\Lambda = m_p/M_p = \rho T_0 \pi r_p^2/M_p$, M_p is the total mass of puncture head and its applied load.

According to impact energy from drop-tower testing, the initial puncture velocity is:

$$E1 = \frac{1}{2} M_p V_p^2 \Rightarrow V_p = \sqrt{\frac{2E1}{M_p}} \tag{5}$$

where $E1$ is the first level of stab-resisting protection.

Combined with equations (4) and (5), the velocity of compound fabric after contacting with puncture head was:

$$V_{p0} = \frac{\sqrt{2}}{1+\Lambda}\sqrt{\frac{E1}{M_p}} \tag{6}$$

(2) Deformation Process

On the hypothesis of $t=t_a$, the compound fabric reached the maximum deformation and then the maximum dynamic puncture force $F'_{\max}$. According to the law of conservation

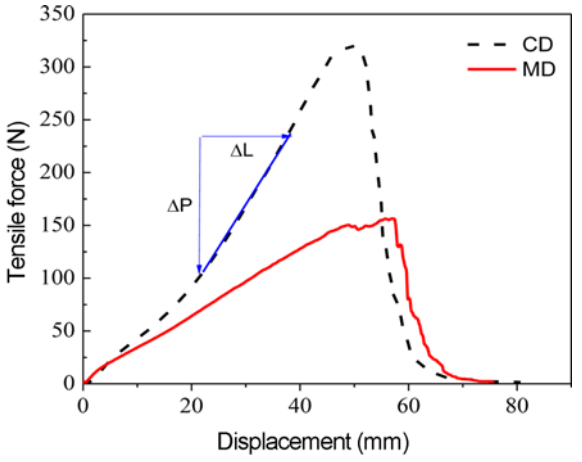

Figure 8. Tensile behaviors of compound fabrics along machine direction and cross direction.

of energy, it is expressed as:

$$\frac{1}{2}M_pV_{p0}^2=\frac{1}{2}M_pV_{p1}^2+E_{DE} \tag{7}$$

where E_{DE} is the deformation energy of compound fabrics.

As displayed in Figure 8, the initial tensile behavior presents the linear regardless of machine direction and cross direction. Therefore, the compound fabrics are assumed to be deformed following elastic behavior, the tensile deformation energy at strain ε is defined as:

$$E_{DE}=\frac{1}{2}M\varepsilon^2 \tag{8}$$

The total energy absorbed by deformation zone can be obtained by [15]:

$$E_{DE}=T\int_{D/2}^{R}\frac{1}{2}M2\pi 2\cdot dr\cdot 4\varepsilon_0^2\left(\frac{R_c-r}{2R_c-D}\right) \tag{9}$$

where M shows the tensile modulus of the compound fabric.

Therein,

$$R_c=\frac{D}{2}+ut_a \tag{10}$$

where u shows the approximate value for transverse wave speed as suggested by reference [17].

(3) The penetration through compound fabric process

The puncture head penetrated through surface of compound fabric after elapsing by t_b, and the velocity of the puncture was V_m. Based on conservation of momentum, it is:

$$M_pV_{p1}-F'_{\max}t_b=M_pV_m \tag{11}$$

After penetration through compound fabric, the puncture velocity is consumed by elastic energy by a spring. Therefore,

$$\frac{1}{2}M_pV_m^2=\frac{1}{2}kx^2\Rightarrow V_m=\sqrt{\frac{k}{M_p}}x \tag{12}$$

Where k is elastic coefficient (47.14 N/m), and x is the compressed length of spring.

Combined with equations (11) and (12), it is expressed as:

$$M_pV_{p1}-F'_{\max}t_b=M_p\sqrt{\frac{k}{M_p}}x \tag{13}$$

Comparisons of Modeling and Experiment Results

After parameters in Table 3 are substituted into equations (7), (9), (10), (13), the results of modeling and experimental for compound fabrics with different kinds of fabrics are displayed in Table 4. It is found that the predicted dynamic puncture resistance of G-CF was in the scope of experimental values, and the modeling result only has the difference of 9.5 % from the mean experimental value. However, the differences between them for K-CF and G-CF are smaller, 4.5 % and 3.55 % respectively. Therefore, the modeling can be predicted the dynamic puncture force of thermal-bonded compound fabrics very well.

Table 3. Yarn density, modulus and elongation of compound fabrics

Yarn	Fineness	Density (g/cm^3)	Diameter (mm)	Tensile strength (GPa)	Modulus (GPa)	Elongation (%)
Glass	1100 D	2.55	0.25	2	73	2
Carbon	12 K	1.78	3.40	1.4	240	1.4
Kevlar	1000 D	1.45	0.31	2.76	124	2.5

Table 4. Predicted and experimental values of dynamic puncture force

Compound fabrics	Areal weight (g/m^2)	E (GPa)	ε_0 (%)	Thickness (mm)	t_a (ms)	t_b (ms)	x (mm)	$\overline{F'_{\max}}$ (N)	$F'_{\max}$ (N)
G-CF	701	0.020	50.3	2.06	62.568	47.4	-10.7	63.26	69.972±11.17
K-CF	573	1.376	9	2.08	35.31	46.01	-10.0	85.01	72.47±9.23
C-CF	751	1.652	2.42	2.00	32.579	48.887	-9.10	98.34	82.467±12.90

Table 5. Coefficients of dynamic puncture resistance related to number of layers

Compound fabric	Intercept *B*	B1	B2	Adj. R-square
G-CF	137.93	97.90	37.23	99.15 %
K-CF	315.02	-92.95	72.03	92.65 %
C-CF	-128.74	352.89	-15.16	98.61 %

Optimization of Number of Layers

Different types of reinforced fabrics fabricated various areal weights of compound fabrics. Therefore, dynamic puncture force at per unit volume density was used to characterize the dynamic puncture properties of different compound fabrics. According to Table 5, the dynamic puncture resistance at per volume density (Y) vs. number of layers (X) conforms to parabolic relations, that is,

$$Y = B + B1 * X + B2 * X^2 \quad (14)$$

where B was intercept, B1 was first order of constant, and B2 was two orders of constant. The three parameters in equation (14) have shown in Table 5. It is found that the correlation coefficient reaches above 90 %, confirming the parabolic relations of dynamic puncture resistance and number of layers.

Other than dynamic puncture force, the puncture depth was also used to evaluate the dynamic puncture properties. Based on NIJ- standard, this index is to protect the injurers from trauma. To reach E1 protection level, the puncture depth must be less than 7 mm. The total length of puncture is 7 inch, 177.8 mm. In this experiment, the puncture depth is defined as the distance between original spring and stopping puncture head during the drop-tower puncture testing. If the puncture beam drops on the spring and the spring happened compression deformation, the puncture depth is recorded as negative value; but conversely, if the puncture beam stopped on the elongated spring, it is recorded as positive value (see Figure 9). As shown Figure 9, the elongation of the spring indicates the puncture depth that the length of spike not exposing the bottom of the compound fabrics. That is, the higher the puncture depth, the lower the penetration depth. Penetration depth shows the exposed length of spike after dynamic puncture testing.

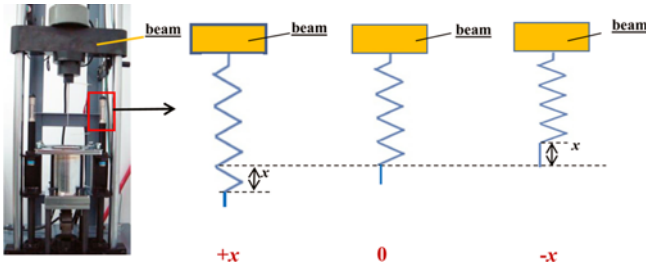

Figure 9. Simplified diagram for puncture depth.

Based on our primary study, the maximum dynamic puncture occurs when the maximum conical radius of spike penetrated through the compound fabrics. Therefore, when the compound fabric reaches the E1 protection level, the puncture depth should be 170.8 mm.

Three types of compound fabrics from one-layer to five-layer are conducted dynamic puncture test. The puncture depth, thickness and areal weight of compound fabrics are respectively determined by the experimental. And then, the fitting relations between them and number of layers are displayed in Figures 10-12.

It is found that puncture depth parabolically increases with number of layers; and the slope rises faster at higher number of layers. This is because much more fabrics dispersed the puncture energy by stress transmission and conical deformation; and also the velocity of compound fabrics becomes smaller after more times of momentum exchange. Evidently, the thickness and areal weight both improve linearly with the number of layers. As shown in Table 6, puncture depth of thermal-bonded C-CF increased more significantly with number of layers, as compared to that of G-CF and K-CF. It is because of the highest elastic modulus

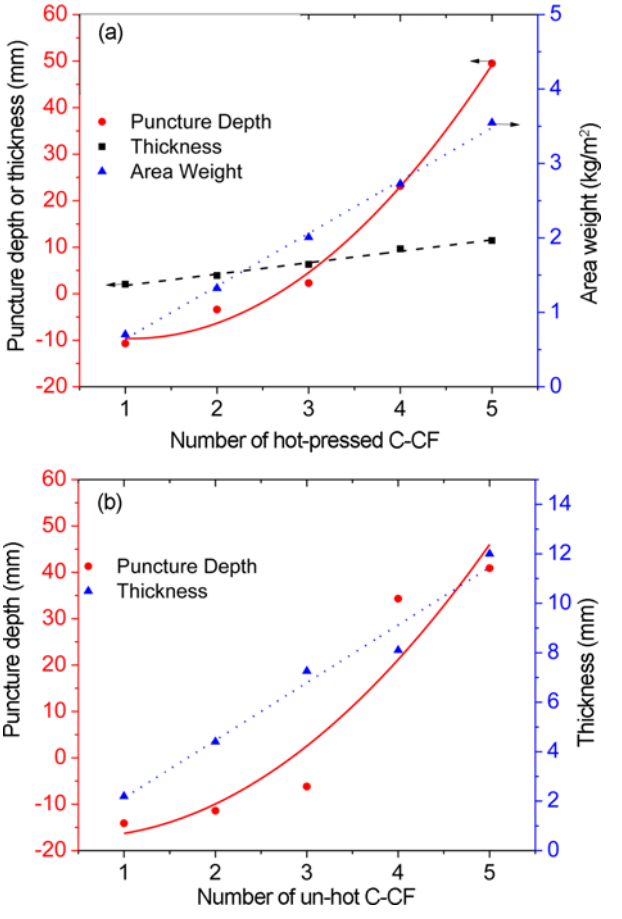

Figure 10. Puncture depth, thickness and area weight of hot-pressed and non-hot-pressed G-CF as related to number of layers.

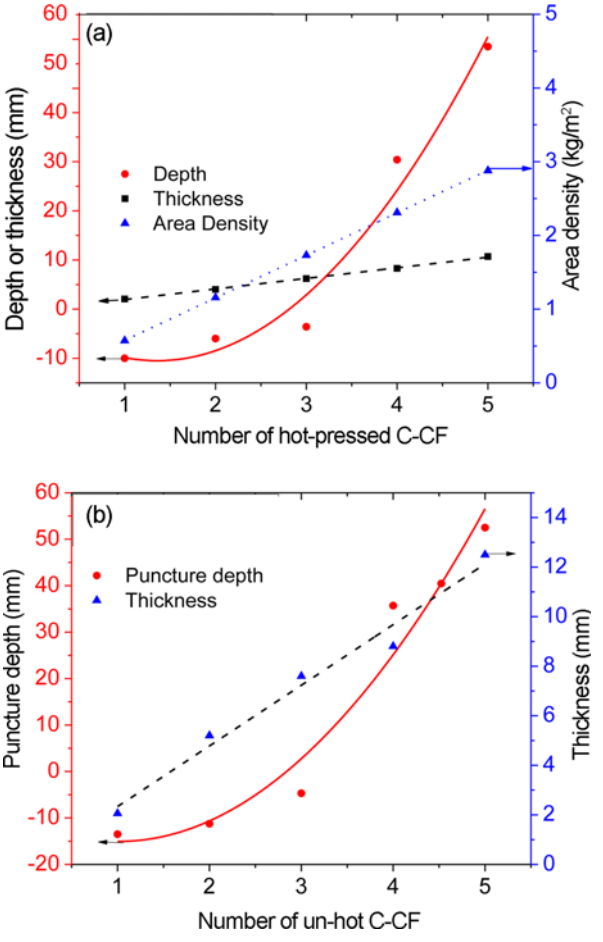

Figure 11. Puncture depth, thickness and area weight of hot-pressed and non-hot-pressed K-CF as related to number of layers.

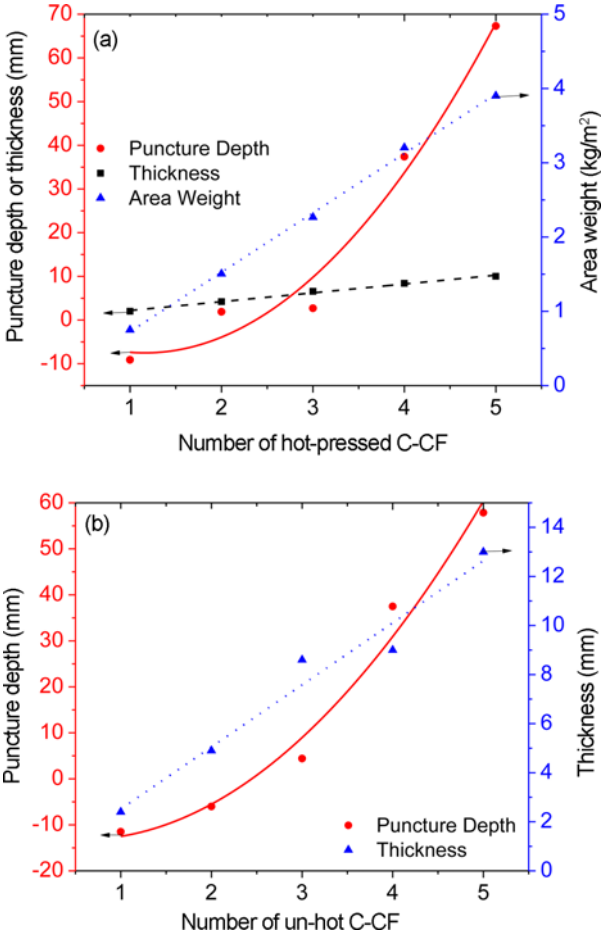

Figure 12. Puncture depth, thickness and area weight of hot-pressed and non-hot-pressed C-CF as related to number of layers.

Table 6. Puncture depth, thickness and area weight of compound fabrics as related to number of layers

Samples group	Characterization index	Relations of Y and X	Adj. R-square (%)
Hot-press G-CF	Puncture depth (mm)	$Y=-5.28-8.13X+3.80\ X^2$	98.738
	Thickness (mm)	$Y=-0.198+2.33X$	96.247
Un-hot G-CF	Puncture depth (mm)	$Y=-16.48-2.87X+3.07\ X^2$	80.18
	Thickness (mm)	$Y=-0.684+2.452X$	98.613
	Weight (g/m^2)	$Y=-66.8+709.2X$	99.643
Hot-press K-CF	Puncture depth (mm)	$Y=-1.32-13.51X+4.97\ X^2$	94.13
	Thickness (mm)	$Y=-0.196+2.152X$	99.834
Un-hot K-CF	Puncture depth (mm)	$Y=-10.46-9.08X+4.49X^2$	89.868
	Thickness (mm)	$Y=-0.112+2.45X$	97.174
	Weight (g/m^2)	$Y=-0.1+576.7X$	99.99
Hot-press C-CF	Puncture depth (mm)	$Y=-0.6-11.89X+5.12\ X^2$	94.974
	Thickness (mm)	$Y=0.176+2.02X$	99.175
Un-hot C-CF	Puncture depth (mm)	$Y=-12.00-4.24X+3.74\ X^2$	96.009
	Thickness (mm)	$Y=-0.01+2.53X$	95.106
	Weight (g/m^2)	$Y=-74.1+799.9X$	99.912

Table 7. Number of layers, thickness and area weight of compound fabric when reaching E1 protective level

Sample code	Number of layers	Thickness (mm)	Area weight (kg/m^2)
Hot-press G-CF	8	18.40	5.6
Un-hot G-CF	8	18.93	5.6
Hot-press K-CF	8	15.73	4.6
Un-hot K-CF	8	17.02	4.6
Hot-press C-CF	8	16.30	6.3
Un-hot C-CF	8	20.23	6.3

of carbon fabric and then larger deformation after dynamic puncture testing. Comparatively, thermal bonding positively affects the puncture depth; that is, thermal-bonded compound fabrics exhibited higher puncture depth as confirmed the rising slope of compound fabrics.

According to these relations in Table 7, eight-layers of compound fabrics reach the E1 protection level, and their thickness and areal weight are displayed in Table 6. At E1 level, the areal weights of G-CF, K-CF and C-CF are 5.6 kg/m^2, 4.2 kg/m^2, 6.3 kg/m^2, which are all lighter than the thermoplastic-impregnated Kevlar fabrics. Compared to three kinds of compound fabrics, K-CF resulted in the more effectively resistance against dynamic puncture. Its thickness is 15.73 mm after being thermal-bonded at E1 protection level. Compared to other flexible woven fabrics made of hybrid yarns [18], the area weight of K-CF is three times lighter than the aramid/cotton woven fabrics, and the thickness is decreased by 10 % of the aramid/cotton woven fabric.

Conclusion

The modeling of dynamic puncture properties with different reinforced fabrics is constructed, and the optimization of number of layers in varying reinforced fabrics is explored simultaneously. The predicted model agrees well with experimental results, and the difference between them is as small as 4.5 % (K-CF) and 3.55 % (C-CF). The modeling result shows that the dynamic puncture resistance is affected by the elastic modulus, conical deformation radius and the thickness of compound fabrics based on maximum deformation and stress-wave transmission theory. With number of layers, the maximum dynamic puncture resistance polynomially improves and penetration depth parabolically decreases. Various kinds of reinforced fabrics affected the dynamic puncture resistance differently as related to number of layers, and penetration depth of C-CF is more significantly affected by number of layers. By numerical analysis, the penetration depth nonlinearly decreases with number of layers, and the minimum safety layer for K-CF is eight. At the E1 protection level, the eight layers of K-CF have the area weight of 4.2 kg/m^2 and a thickness of 15.73 mm. In sum, the predicted model for dynamic puncture resistance in this study is accurate, and provides theoretical supports on the future for designing puncture-resisting body armor. This intra-/inter- reinforced compound fabrics used for body armor have advantages of flexible, light weight and comfortability.

Acknowledgment

The authors acknowledge the financial supports from the National Science Foundation of China (Grant Number 51503145, 51303128 and 51303131).

References

1. J. B. Mayo, E. D. Wetzel, M. V. Hosur, and S. Jeelani, *Int. J. Impact. Eng.*, **36**, 1095 (2009).
2. Y. Termonia, *Int. J. Impact. Eng.*, **32**, 1512 (2006).
3. L. Wang, S. Zhang, W. M. Gao, and X. Wang, *CMES*, **20**, 11 (2007).
4. B. Sun, Y. Wang, P. Wang, and B. Gu, *Text. Res. J.*, **81**, 992 (2011).
5. P. Wang, B. Sun, and B. Gu, *Text. Res. J.*, **82**, 1337 (2012).
6. M. F. Yahya, S. A. Ghani, and J. Salleh, *Text. Res. J.*, **84**, 1095 (2014).
7. W. Barnat, D. Sokołowski, and R. Gieleta, *Fibres Text. East. Eur.*, **22**, 90 (2014).
8. L. Hou, B. Sun, and B. Gu, *Appl. Compos. Mater.*, **20**, 569 (2013).
9. T. T. Li, R. Wang, C. W. Lou, and J. H. Lin, *Text. Res. J.*, **82**, 1597 (2012).
10. R. Wang, T. T. Li, C. W. Lou, J. Y. Lin, and J. H. Lin, *Mater. Manuf. Process.*, **28**, 1029 (2013).
11. T. T. Li, R. Wang, C. W. Lou, J. Y. Lin, and J. H. Lin, *Fiber. Polym.*, **15**, 315 (2014).
12. T. T. Li, R. Wang, C. W. Lou, and J. H. Lin, *Compos. Pt. B-Eng.*, **59**, 60 (2014).
13. T. T. Li, R. Wang, C. W. Lou, C. H. Huang, and J. H. Lin, *Fiber. Polym.*, **14**, 258 (2013).
14. T. T. Li, R. Wang, C. W. Lou, and J. H. Lin, *J. Ind. Text.*, **43**, 247 (2013).
15. M. Mamivand and G. H. Liaghat, *Int. J. Impact. Eng.*, **37**, 806 (2010).
16. S. S. Morye, P. J. Hine, R. A. Duckett, D. J. Carr, and I. M. Ward, *Compos. Sci. Technol.*, **60**, 2631 (2000).
17. S. L. Phoenix and P. K. Porwa, *Int. J. Solids Struct.*, **40**, 6723 (2003).
18. D. T. Tien, J. S. Kim, and Y. Huh, *Fiber. Polym.*, **12**, 808 (2011).